Nuclear Instruments and Methods in Physics Research B 358 (2015) 229–235

Contents lists available at ScienceDirect

Nuclear Instruments and Methods in Physics Research B

journal homepage: www.elsevier.com/locate/nimb

Ion beam irradiation effect on thermoelectric properties of Bi_2Te_3 and Sb_2Te_3 thin films

Gaosheng Fu [a], Lei Zuo [a,b,*], Jie Lian [c], Yongqiang Wang [d], Jie Chen [b], Jon Longtin [a], Zhigang Xiao [e]

[a] Department of Mechanical Engineering, Stony Brook University, Stony Brook, NY 11794, United States
[b] Department of Mechanical Engineering, Virginia Tech, Blacksburg, VA 24061, United States
[c] Department of Mechanical, Aerospace & Nuclear Engineering, Rensselaer Polytechnic Institute, Troy, NY 12180, United States
[d] Materials Science & Technology Division, Los Alamos National Laboratory, Los Alamos, NM 87544, United States
[e] Department of Electrical Engineering, Alabama A&M University, Normal, AL 35762, United States

ARTICLE INFO

Article history:
Received 23 January 2015
Received in revised form 22 June 2015
Accepted 28 June 2015

Keywords:
Thermoelectric
Ion beam radiation
Bismuth telluride
Antimony telluride
Thin film

ABSTRACT

Thermoelectric energy harvesting is a very promising application in nuclear power plants for self-maintained wireless sensors. However, the effects of intensive radiation on the performance of thermoelectric materials under relevant reactor environments such as energetic neutrons are not fully understood. In this work, radiation effects of bismuth telluride (Bi_2Te_3) and antimony telluride (Sb_2Te_3) thermoelectric thin film samples prepared by E-beam evaporation are investigated using Ne^{2+} ion irradiations at different fluences of 5×10^{14}, 10^{15}, 5×10^{15} and 10^{16} ions/cm^2 with the focus on the transport and structural properties. Electrical conductivities, Seebeck coefficients and power factors are characterized as ion fluence changes. X-ray diffraction (XRD) and transmission electron microscopy (TEM) of the samples are obtained to assess how phase and microstructure influence the transport properties. Carrier concentration and Hall mobility are obtained from Hall effect measurements, which provide further insight into the electrical conductivity and Seebeck coefficient mechanisms. Positive effects of ion irradiations from Ne^{2+} on thermoelectric material property are observed to increase the power factor to 208% for Bi_2Te_3 and 337% for Sb_2Te_3 materials between fluence of 1 and 5×10^{15} cm^2, due to the increasing of the electrical conductivity as a result of ionization radiation-enhanced crystallinity. However, under a higher fluence, 5×10^{15} cm^2 in this case, the power factor starts to decrease accordingly, limiting the enhancements of thermoelectric materials properties under intensive radiation environment.

1. Introduction

Thermoelectric generator allows the direct solid-state conversion between thermal and electrical energy [1], which are of particular interest for waste heat recovery [2], improved energy efficiency [3], and powering of remote sensors and electronics [4]. Among the many potential applications, thermoelectrics for power harvesting in nuclear power plants for sensors and sensing networks are especially attractive since heat is available at a variety of locations.

Nuclear plants accidents (Chernobyl, Three Mile Island, and Fukushima Daiichi) have casted a shadow on the history and future of nuclear power. Safety thus rightfully remains an enormous concern in the development and operations of nuclear power plants and fuel cycles. In the Fukushima event, one major concern was a total loss of power at the plant, leading to catastrophic failure of reactor systems and loss of coolants. As a result, sensing and actuation systems stopped working. Increasingly research is going on recently to develop thermoelectric-driven sensing technologies to power sensor and communication packages in the event of massive power loss. Lin et al. [5] discussed the development of an independently powered sensor network that uses thermoelectric generators (TEGs) to provide power for monitoring and actuation in blackout situations for small modular reactors. Carstens et al. [6] proposed using TEGs to power wireless sensors to monitor spent nuclear fuel during dry-cask storage. Clayton et al. [7] developed and demonstrated an advanced, multifunctional, power-scavenging sensor network system for nuclear power plants.

Several recent studies have reported on the radiation effect on thermoelectric material, thermoelectric module and related power electronics. Back to 1960s, Corelli et al. [8] reported the radiation from the spent fuel can affect the physical properties of the

* Corresponding author.
E-mail address: leizuo@vt.edu (L. Zuo).

http://dx.doi.org/10.1016/j.nimb.2015.06.039
0168-583X/

thermoelectric materials, which then influence the power production from the TEG. At 1961, Kilp et al. [9] reported, when the thermoelectric material was irradiated at reactor ambient temperatures, increase of electrical resistivity and Seebeck coefficient but overall reduction of the power factor. Carstens et al. [6] reported gamma radiation effect on the commercial Hi-Z modules in which they used bismuth telluride based alloy and DC–DC converters. The results showed that TEG was not affected by gamma radiation at a dose rate of 170 Rad/min; while DC–DC converter could not operate normally at the presence of gamma radiation. Up to now, few researchers studied neutron radiation effects on thermoelectric materials.

However, high neutron dose radiation test is not practical due to limited neutron irradiation access as well as the complexity of post irradiation testing. As an alternative investigation method, ion beam irradiation has been used to simulate the radiation damage caused by primary knocked atoms (PKA) upon the interaction of energetic neutrons with materials. Due to the higher and more controllable ion dose rate, the radiation experiment can be completed in a much shorter period due to much higher damage efficiency of energetic ion beams as compared with neutrons. The radiation damage level in terms of displacements per atoms can be simulated using SRIM codes, allowing simulation of radiation damages of the primary knocked atoms (PKAs) upon energetic neutron-atoms interaction. The properties changes of materials can be correlated with the displacement damage levels.

Among the few research work of ion radiation on thermoelectric, Kubiak et al. [10] reported effect of 350 eV He^+, Ar^+ and Xe^+ bombardment of PbTe. They concluded in the case of Ar^+ and Xe^+ bombardment the altered layer appears to extend over a depth commensurate with the ion range, the results for He^+ bombardment suggest that only the very surface is depleted of Te. Budak et al. [11,12] reported MeV Si ion beam modification effects on the thermoelectric generator from $Er_{0.1}Fe_{1.9}SbGe_{0.4}$ and SiO_2/SiO_2 + Ge nanolayers thin film. Guner et al. [13] studied effects of MeV Si ions bombardment on the thermoelectric properties of Zn_4Sb_3 and $CeFe_2Co_2Sb_{12}$ thin films. Zheng et al. [14,15] reported improvement on thermoelectric properties of multilayered multilayer super-lattice by MeV Si ion beam bombardment.

In this work, the properties of thin films Bi_2Te_3/Sb_2Te_3 grown using e-beam evaporation and irradiated using Ne^{2+} ion are reported. Structural properties for ion beam irradiated Bi_2Te_3/Sb_2Te_3 thin films are presented. Also, the influence of Ne^{2+} ion fluence level on crystallinity and defect accumulation for both samples are discussed. Measurements of electrical conductivity, Seebeck coefficient, carrier concentration and mobility are performed on ion bombarded samples with different fluences. For reference as-grown thin films are also characterized and compared to the ion-bombarded samples. An ionization radiation-induced defect recovery and reorientation were observed for both films as evidenced by XRD and TEM. A competition of the ionization radiation and displacement damage dominates the variations of the electrical and thermoelectrical properties of materials. Positive effects of ion irradiations from Ne^{2+} on thermoelectric materials are observed, which increases the power factors of Bi_2Te_3 and Sb_2Te_3 materials, respectively, consistent with the increase of the electrical conductivity as a result of ionization radiation-enhanced crystallinity.

2. Experiment and methods

Thermoelectric performance is characterized by the dimensionless figure of merit $ZT = \sigma S^2 T/k$ and power factor $PF = \sigma S^2$ where S is the Seebeck coefficient (V/K), σ is the electrical conductivity (S/m), k is the thermal conductivity (W/m K), and T is the absolute temperature in Kevin (K). The electrical conductivity $\sigma = ne\mu$ is given by carrier concentration n carrier mobility μ and electron charge e Carrier concentration and mobility can be determined by measuring the Hall coefficient R_H. For materials in which electrons are the primary carriers, $R_H = -1/ne$. Combining the Hall effect coefficient and electrical conductivity, the mobility of such materials can be expressed as $\mu = -\sigma R_H$. An expression for the Seebeck coefficient for n-type thermoelectric material is obtained by Busch and Winkler [16] as.

$$S = -\frac{k}{e}\left(\frac{5}{2} + r - \ln\frac{n}{N_c}\right). \quad (1)$$

here k is Boltzmann's constant, r is the exponent of the power function in the energy-dependent relaxation time expression [17], and N_c is the effective density of states in the valence band. As can be seen, the Seebeck coefficient is affected by carrier concentration, n. Three-inch-diameter boron-doped p-type <1 0 0> silicon wafers (Montoco Silicon Technologies, Inc.) are used as the substrates in this research. The silicon wafers are 350- to 400-μm-thick and the resistivity is in 1–5 Ω cm range. The wafers are initially oxidized at 1100 °C for 60 mins to get a 0.5-μm-thick silicon dioxide layer using wet thermal oxidation. The Bi_2Te_3 and Sb_2Te_3 thin films are grown by e-beam evaporation deposition, using a Kurt J. Lesker PVD 75 E-beam/thermal evaporation system. Solid antimony (III) telluride and bismuth (III) telluride (99.999% purity; Alfa Aesar Company) are evaporated for growth of the Bi_2Te_3 and Sb_2Te_3 thin films, respectively. The films are deposited at room temperature without substrate heating. The process chamber has a background pressure of 2×10^{-7} Torr. The thickness of Bi_2Te_3 and Sb_2Te_3 thin films is controlled by an INFICON deposition monitor during the deposition, and measured by Stylus Profilometry (Bruker, IL, USA). Table 1 summarizes all of the samples grown by e-beam evaporation and ion beam irradiation conditions.

The ion beam irradiations on thin film samples are performed at Ion Beam Lab of Los Alamos National Laboratory with 0.4 MeV Ne^{2+} ions using a 200 kV ion implanter. The ion irradiation is performed at room temperature without sample titling, and the samples are irradiated at different fluences from 0.5×10^{15}, 1×10^{15}, 5×10^{15} and 10×10^{15} ions/cm^2. The ion fluences are also converted to the unit of displacements per atom (dpa) using the Stopping and Range of Ions in Matter (SRIM)-2008 program based on the Kinchin-Pease model and full cascade calculations (Table 1) using a displacement energy of 25 eV for every atom.

The displacement energy is 25 eV for all of the elements in Bi_2Te_3 and Sb_2Te_3. The ion ranges of the 400 keV Ne^{2+} in thermoelectric thin films were 493 nm for Bi_2Te_3 and 520 nm for Sb_2Te_3, respectively, significantly larger than that of the film thickness (see Table 2). These results suggest that most of the implanted Ne^{2+} penetrated through the film thickness such that the chemical effort on the electrical and thermoelectric properties of the films

Table 1
Sample synthesis method, ion fluence and displacements per atoms (dpa) based on SRIM-2008 calculation.

Sample	Material	Condition	Ion fluence (10^{15} ions/cm^2)	dpa
N0	Bi_2Te_3	E beam	0	0
P0	Sb_2Te_3	E beam	0	0
N1	Bi_2Te_3	E beam + ion beam	0.5	0.09
N2	Bi_2Te_3	E beam + ion beam	1	0.19
N3	Bi_2Te_3	E beam + ion beam	5	0.93
N4	Bi_2Te_3	E beam + ion beam	10	1.87
P1	Sb_2Te_3	E beam + ion beam	0.5	0.07
P2	Sb_2Te_3	E beam + ion beam	1	0.15
P3	Sb_2Te_3	E beam + ion beam	5	0.74
P4	Sb_2Te_3	E beam + ion beam	10	1.49

Table 2
Ion irradiation parameter, ion range, electronic and nuclear energy loss and the ratio of the ENSP as evaluated by full cascade calculation based on SRIM-2008.

Materials	Thickness (nm)	Ion sources	S_e (eV/nm)	S_n (eV/nm)	ENSP	Ion range (nm)
Bi_2Te_3	160	400 keV Ne^{2+}	617	125	4.9	493
Sb_2Te_3	100	400 keV Ne^{2+}	595	106	5.6	520

can be neglected. In addition, the electronic energy S_e, nuclear energy loss S_n and the ENSP (electron to nuclear stopping power ratio) were estimated based on the average value across the depth of the thin film samples and the full cascade calculations of SRIM-2008.

The phase composition of the samples before and after irradiations was analyzed with X-ray diffraction (XRD) (Ultimate III, Rigaku, TX, USA) utilizing Cu Kα radiation and energy-dispersive X-ray spectroscopy (EDS) (JEOL 7600F, Tokyo, JP). The cross-section morphologies of the sample were observed using a transmission electric microscope (TEM) (JEOL 1400, Tokyo, JP). The electrical conductivity was measured using a Keithley digital multimeter (Model 2700, Keithley Instruments, Inc., OH, USA) and heated from 300 to 400 K using a High Temperature Probe Station (MBE-Komponenten AO500, Germany). Seebeck coefficients were measured using a differential method under vacuum. To investigate its contribution to electrical conductivity, the carrier concentration and Hall mobility were measured with a Hall Measurement System (8404, Lake Shore Cryotronics, Inc., OH, USA) using the Van der Pauw method.

3. Results and discussions

3.1. Phase composition of Bi_2Te_3 and Sb_2Te_3 before and after ion beam irradiation

Fig. 1 shows the XRD patterns of Bi_2Te_3 and Sb_2Te_3 thin films before and after ion bombardment. Sample N0 and P0 were as-grown *n*-type Bi_2Te_3 and *p*-type Sb_2Te_3 samples using e-beam evaporation; while the rest samples were bombarded with Ne^{2+} ion at different total fluences. For Bi_2Te_3, the as-grown thin film showed main phase orientation at direction (015). Upon 400 keV Ne ion irradiation, no irradiation-induced amorphization was observed, and both Bi_2Te_3 and Sb_2Te_3 samples remain highly crystalline as revealed by the XRD patterns. The increase in the ion fluence will further increase the crystallinity as evidenced by the peak narrowing of the XRD patterns. Additionally, an irradiation-induced reorientation occurred for both thin films, as evidenced by the increased intensity of the XRD diffraction peaks of (006) and (0015) for Bi_2Te_3 (Fig. 1a). A similar behavior was observed for Sb_2Te_3 film (see Fig. 1b). Before ion beam irradiation, the as-grown sample is located at mainly (015) direction and after the irradiation secondary preferred orientation in the direction of (009) is clearly visible as ion fluence increases.

The energy loss mechanism of the energetic ions is crucial in determining the irradiation damage process. The ballistic effect of nuclear energy loss (or nuclear stopping power: S_n) causes atomic displacements that can lead to amorphization of the irradiated materials. On the other hand, ionization radiation can promote defect recombination or recovery, even recrystallization of materials. A higher ENSP (electron to nuclear stopping power ratio) value may result in higher radiation defect recovery rate as compared with radiation damage accumulation, and hence enhanced radiation resistance. The radiation-enhanced crystallinity and reorientation of the thermoelectric thin films upon 400 keV Ne^{2+} suggests that the ionization radiation dominated radiation damage process. This is consistent with the relatively small displacement damage created by the Ne^{2+} ions even at the highest ion fluences (1.87 and 1.49 dpa for Bi_2Te_3 and Sb_2Te_3, respectively), and significantly higher electronic energy loss Se and greater ENSP ratios for both Bi_2Te_3 and Sb_2Te_3. The ionization-radiation enhanced crystallinity and reorientation may also lead to the reduction of the defects upon irradiation and thus increases in the electrical conductivity upon initial ion irradiation as elaborated later.

3.2. TEM of Bi_2Te_3 and Sb_2Te_3 before and after ion beam irradiation

Fig. 2 shows the TEM images and diffraction patterns of two type samples before and after ion irradiation. The Fig. 2(a) shows a high magnificent TEM of as grown Bi_2Te_3 and Fig. 2(b) shows the TEM of Bi_2Te_3 after 5×10^{15} ions/cm^2 ion radiation N3 sample. As shown, the grain size increases in N3 suggesting the ionization radiation-induced defect recovery and grain growth, consistent with the XRD patterns. The selected electron diffraction pattern (SAED) of the as-grown Bi_2Te_3 film (inset in Fig. 2a) shows a ring

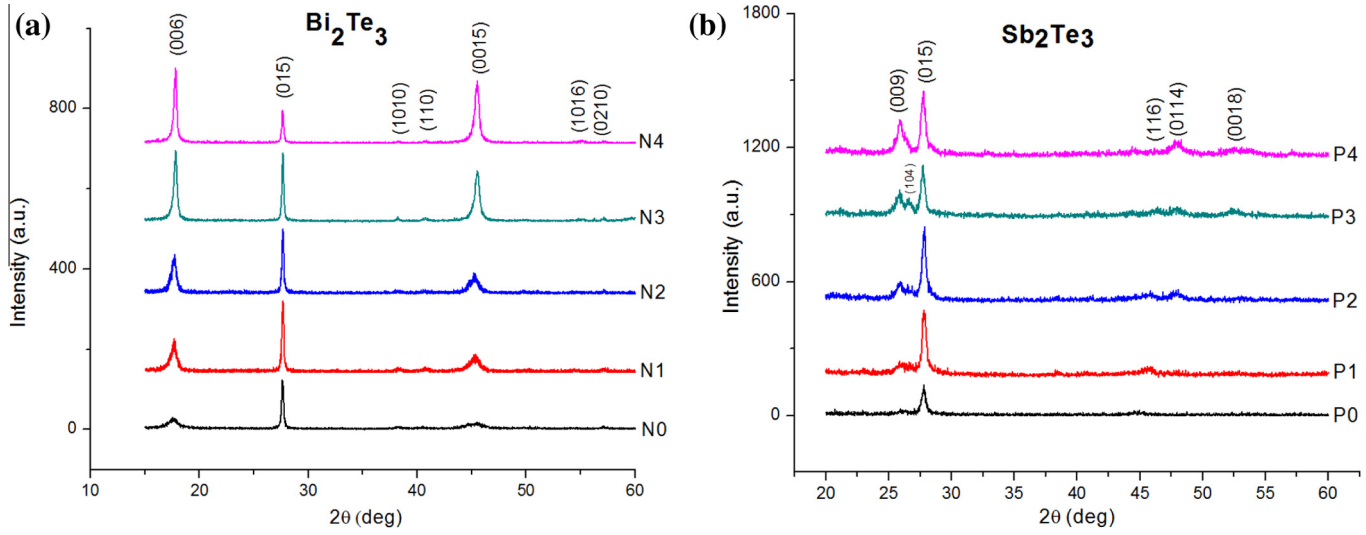

Fig. 1. XRD of Bi_2Te_3 (a) and Sb_2Te_3 (b) thin film before and after ion beam irradiation shows an irradiation-induced reorientation and enhancement of crystallinity as the ion fluence increases.

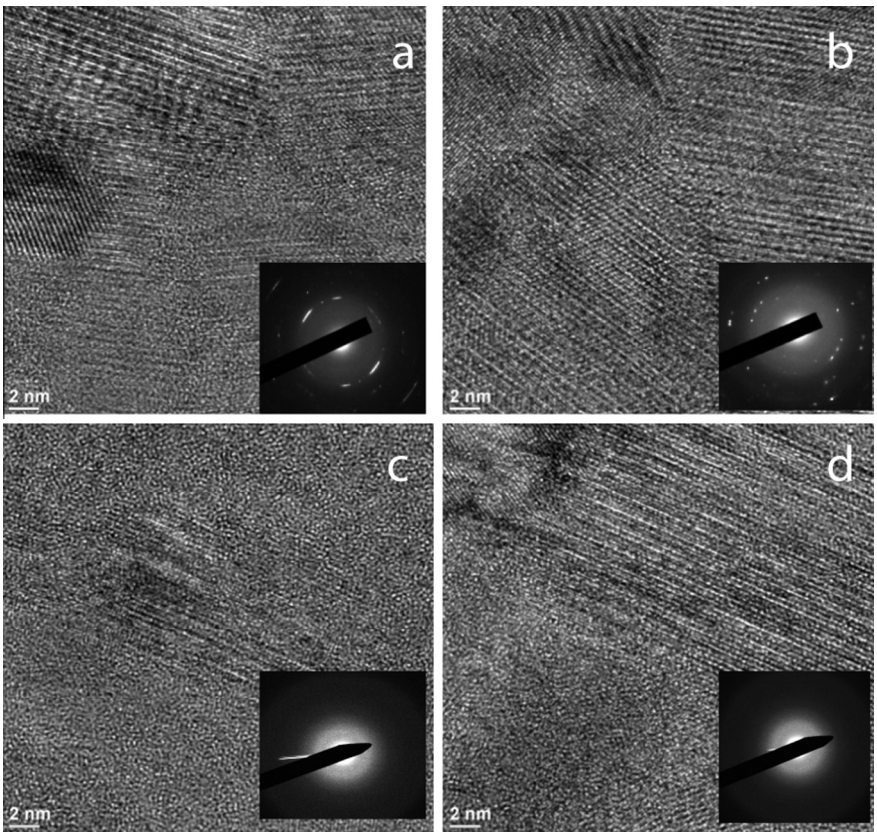

Fig. 2. TEM of Bi_2Te_3 (a) before radiation N0, (b) after radiation N3 and Sb_2Te_3 (c) before radiation P0, (d) after radiation P3.

pattern, a characteristic feature of the nanocrstyalline materials. A preferred orientation was observed as shown by the arc in the SAED which can be indexed as the (0 1 5) spacing based on structural data of Bi_2Te_3 (PDF#15-0874). Upon ion irradiation, the SAED pattern consists of discrete diffraction spots, inferring increased grain size upon ion irradiation. The originally preferred orientation of the (0 1 5) disappeared despite radiation-induced reorientation was observed, probably due to the different zone axis of the SAED pattern. Similar behavior occurred for Sb_2Te_3 film upon irradiation. Before irradiation, the Sb_2Te_3 thin film has a low degree of crystallinity, and nano-sized particles were embedded into an amorphous-dominated matrix (Fig. 2c). The selected electron diffraction pattern (SAED) of the as-grown Sb_2Te_3 film (inset in Fig. 2c and d) also shows a low degree of crystallinity. Ion irradiation significantly improves the crystallinity of the material as a result of the ionization radiation-induced defect recovery process. Overall, N type Bi_2Te_3 sample has better crystallinity than P type Sb_2Te_3 and TEM results are well correlated with XRD results showed before. The orientation changes after ion radiation implies the randomization happens during the process.

3.3. Transport properties of Bi_2Te_3 and Sb_2Te_3

3.3.1. Electrical conductivity variation upon ion irradiation

Electrical resistivity measurements were made from 300 to 400 K under vacuum. The measured electrical conductivities for both samples are shown in Fig. 3, which indicates that the variation in electrical conductivity is significant upon ion radiation. In Fig. 3(a), N0 which was as-grown sample, has a slightly higher resistivity than the rest Bi_2Te_3 samples with ion beam irradiations. For the Sb_2Te_3 thin film sample, the trend is similar as Bi_2Te_3 sample: P0 has higher electrical resistivity than P1–P4 upon ion beam irradiation, which is again likely due to the radiation induced ionization during ion radiation process. The decrease of electrical resistivity of both samples with increase of temperature is of the intrinsic semiconductor character.

Fig. 4 shows the variation of the electrical conductivity as a function of ion fluence. For both films, the as-grown samples have higher resistivities than the materials after ion beam irradiation, consistent with lower carrier concentration as referred from Hall Effect measurements (Table 3). The improved electrical conductivity of both films with increased fluences may be attributed to the ionization-induced recovery of the intrinsic defects during film deposition process, and thus enhancement of the carrier concentration. With further increase of ion fluence above 5×10^5 ions/cm^2, the electrical conductivity decreases for both N4 and P4 samples as a result of the accumulation of displacement-induced defects in the thin film in which the displacement damage dominates over the ionization radiation.

In order to understand the mechanisms and key parameters that affect electrical conductivity, Hall effect measurements at room temperature were made with van der Pauw method and the results are shown in Table 3. The as-grown Bi_2Te_3 and Sb_2Te_3 thin film (N0 and P0) have lower carrier mobility than those of ion beam irradiated samples. As ion fluence increases before 5×10^{15} ions/cm^2, the carrier mobility in both Bi_2Te_3 and Sb_2Te_3 sample increases due to radiation induced defect recovery process showed in XRD result (see Fig. 1). After the ion fluence reaches 5×10^{15} ions/cm^2, higher fluence starts to decrease the mobility which may come from the accumulated defects generated by ion radiation. In Table 3, the carrier concentration of the Bi_2T_3 and Sb_2Te_3 samples starts to decrease at the beginning of ion radiation and it turns reversely at higher fluence. The carrier concentration

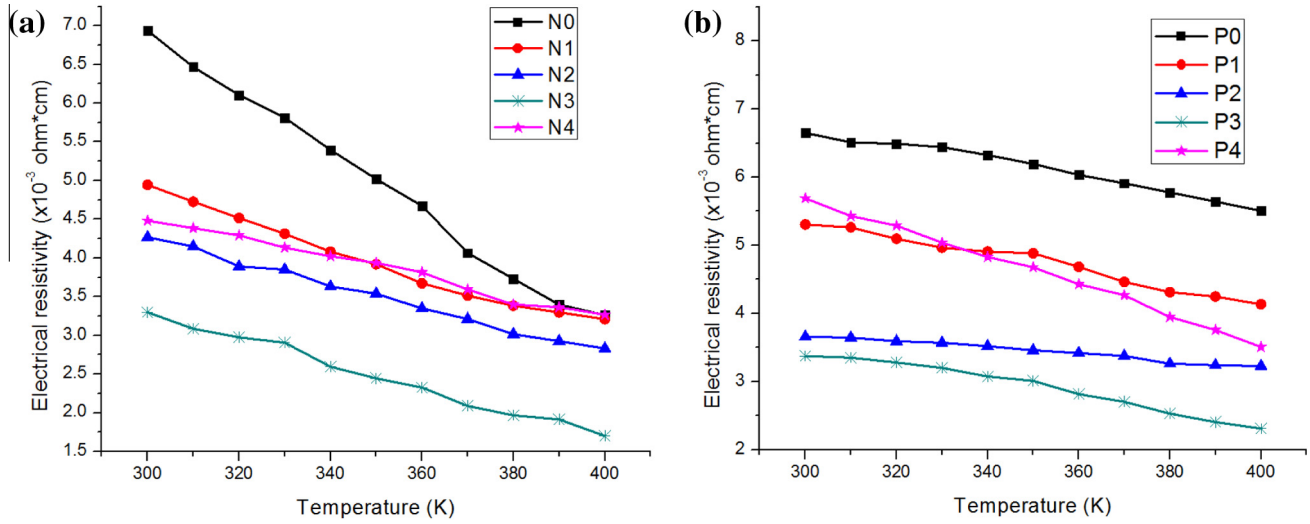

Fig. 3. Electrical resistivities of Bi_2Te_3 (a) and Sb_2Te_3 (b) thin film after bombardment decrease to some extent and then increase after the ion fluence of 5×10^{15} ions/cm^2.

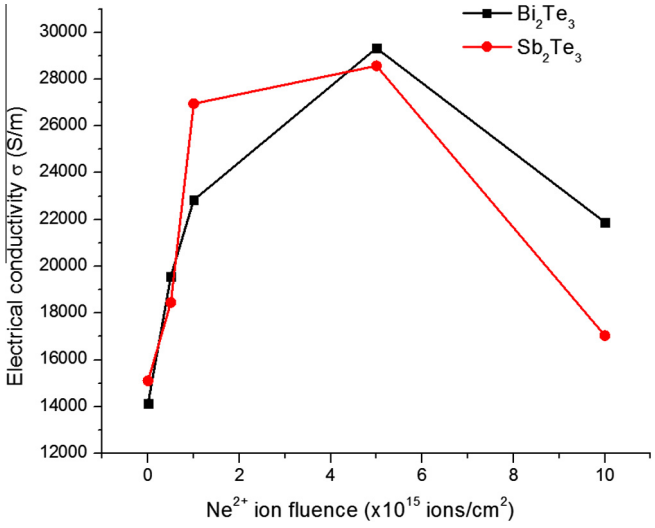

Fig. 4. Room temperature electrical conductivity for Bi_2Te_3 and Sb_2Te_3 samples at various ion fluences.

by Hall effect measurements matches well with the electrical resistivity using four-probe machine at room temperature. The change of the carrier concentration may also be associated with the mini-bands formation during ion radiation process.

The samples in this study are non-stoichiometric and polycrystalline. The mobility is far less than that of stoichiometric Bi_2Te_3/Sb_2Te_3 single crystal, e.g., mobility of 313 cm^2/V sec for thin films Bi_2Te_3 using metalorganic chemical vapor deposition [18] and 400 cm^2/V sec for single crystal bulk Sb_2Te_3 [19]. Generally, mobility is determined by phonon scattering at high temperatures and ionized impurity scattering at low temperatures for semiconductor materials [20]. For our samples, the increase of crystallization shown in XRD account for the increase of mobility and at higher fluence the accumulated defects decreased the mobility.

3.3.2. Seebeck coefficient

Fig. 5 shows the measured Seebeck coefficients of Bi_2Te_3 and Sb_2Te_3 thin films before and after bombardment. Seebeck coefficient is very sensitive to carrier concentration and inversely proportional to electrical conductivity due to the opposite

Table 3
Room temperature Hall Effect for two type thin film at different fluence.

Sample	Carrier concentration n (10^{20} cm^3)	Hall mobility μ (cm^2/V·s)	Conductivity $\sigma = ne\mu$ (S/m × 10^5)
N0	5.78	1.50	1.4
N1	5.45	2.20	1.9
N2	5.11	2.74	2.3
N3	5.46	3.29	2.9
N4	5.04	2.66	2.2
P0	3.31	2.80	1.5
P1	3.23	3.50	1.8
P2	3.03	5.46	2.7
P3	3.18	5.50	2.8
P4	3.25	3.21	1.7

dependence of carrier concentration, i.e., $S \sim \ln(n)$ in Eq. (1) [16]. Fig. 5(a) shows that the un-irradiated sample N0 has a lower Seebeck coefficient because of its higher carrier concentration. As ion fluence increases from N0 to N2, the Seebeck coefficient increases since the carrier concentration continues to decrease. Fig. 5(b) shows the similar trends for Sb_2Te_3 samples as P0 has a much higher carrier concentration than P1–P4. Generally as temperature increases, the Seebeck coefficient will increase in magnitude because the ratio N_c/n in Eq. (1) is proportional to $\exp(kT)$. The fact that the Seebeck coefficient is negative in Fig. 5(a) indicates that Bi_2Te_3 is an n-type semiconductor, and the positive Seebeck value in Fig. 5(b) shows Sb_2Te_3 is a p-type semiconductor. This observation is consistent with the Hall effect measurement.

3.3.3. Power factor (PF)

The power factor value $PF = S^2\sigma$ of the sample can be estimated by combining the in-plane electrical properties σ and the in-plane Seebeck coefficient S. Fig. 6 shows the in-plane power factors for Bi_2Te_3 and Sb_2Te_3 thin films before and after ion irradiation. Positive effects of ion irradiations from Ne^{2+} on thermoelectric material property are observed because of large improvements in electrical conductivity and Seebeck coefficient caused by carrier concentration and mobility change. Fig. 6 shows the maximum PF for Bi_2Te_3 appeared at 5×10^{15} ions/cm^2 Ne ion fluence, which increased to 208% compared with sample before ion radiation. For Sb_2Te_3 the maximum PF occurred at 1×10^{15} ions/cm^2 Ne^{2+}, which increased to 337% compared with sample before radiation. However, under a higher fluence, 5×10^{15} ions/cm^2 for Bi_2Te_3 and 1×10^{15} ions/cm^2 for Sb_2Te_3, the power factor start to decrease

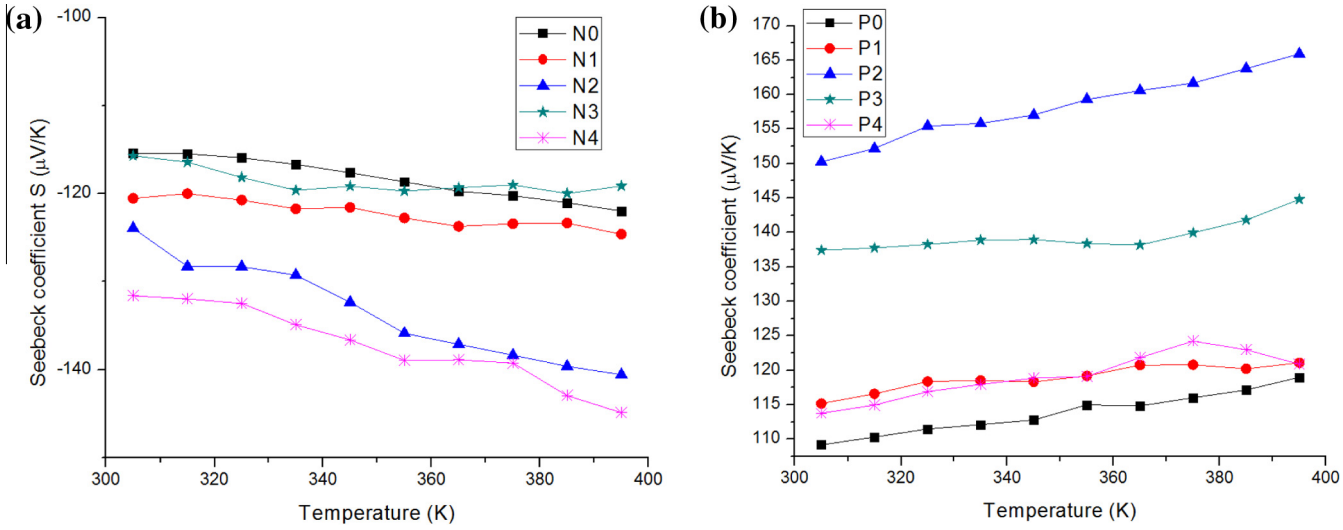

Fig. 5. Seebeck of Bi_2Te_3 (a) and Sb_2Te_3 (b) thin film before and after bombardment.

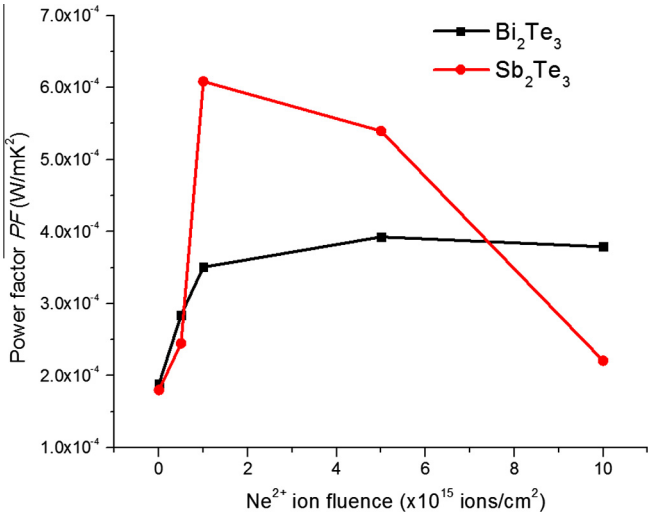

Fig. 6. Room temperature PF of Bi_2Te_3 and Sb_2Te_3 thin film increases when ion fluence increases and the peak achieves between 1×10^{15} ions/cm^2 and 5×10^{15} ions/cm^2.

accordingly, limiting the enhancements of thermoelectrical materials properties under intensive radiation environment. This is because at higher fluence, the mobility becomes smaller as the accumulation of defects generated by displacement damages to the materials and eventually the electrical conductivity starts to decrease.

4. Conclusions

In conclusion, thermoelectric Bi_2Te_3 and Sb_2Te_3 thin films prepared by E-beam evaporation were irradiated by 400 keV Ne^{2+} in order to investigate the radiation effects of the thermoelectrical materials as energy harvester in nuclear environment. The microstructure evolution, phase/crystallinity and the thermoelectrical properties were systematically investigated. An ionization radiation-induced defect recovery and reorientation were observed for both films as evidenced by XRD and TEM. A competition of the ionization radiation and displacement damage dominates the variations of the electrical and thermoelectrical properties of materials. The electrical resistivity decreases in both materials upon ion irradiation due to the increase in carrier mobility and better crystallinity. The accumulated defects induced by displacement damage at higher ion fluence eventually result in the reduction of the mobility and electrical conductivity. Seebeck coefficient increases accordingly with ion radiation due to the reduction of carrier concentration and the charge mobility. Positive effects of ion irradiations from Ne^{2+} on thermoelectric materials are observed, which increases the power factors to 208% for Bi_2Te_3 and 337% for Sb_2Te_3 materials, respectively, consistent with the increase of the electrical conductivity as a result of ionization radiation-enhanced crystallinity. However, under a higher fluence, the power factor starts to decrease, limiting the enhancements of thermoelectrical material properties under intensive radiation environment.

Acknowledgments

The authors gratefully acknowledge financial supports from the DOE Nuclear Engineering University Program CFP-13-5479, CFP-12-3331 and National Science Foundation under the awards CBET #1048744 and DMR #1151028. Research carried out in part at the Center for Functional Nanomaterials, Brookhaven National Laboratory, which is supported by the U.S. Department of Energy, Office of Basic Energy Sciences, under Contract No. DE-AC02-98CH10886. Ion beam irradiation was conducted at ion beam lab at Los Alamos National Laboratory under the support of a CINT (Center for Integrated Nanotechnologies) user proposal (#C2013B0055). The authors wish to thank Dr. Ming Lu, Dr. Xiaoya Shi, Dr. Fernando Camino, Dr. Kim Kisslinger and Mr. James Kierstead from Brookhaven National Laboratory and Mr. Shuyu Wang and Mr. Shifeng Yu from Stony Brook University for help in characterizing the samples. Special thanks go to Dr. Richard Gambino and Dr. Daryush Ila for the insightful discussions.

References

[1] C. Wood, Rep. Prog. Phys. 51 (1988) 459.
[2] G.J. Snyder, E.S. Toberer, Nat. Mater. 7 (2008) 105.
[3] L.E. Bell, Science 321 (2008) 1457.
[4] J.A. Paradiso, T. Starner, IEEE Pervasive Comput. 4 (2005) 18.
[5] J.P. Longtin, in ASME Heat Transfer Summer Conference, Minneapolis, Minnesota, USA, 2013.
[6] T. Carstens, M. Corradini, J. Blanchard, Z. Ma, Electrical and Power Engineering Frontier 2 (2013) 7.
[7] D. Clayton, in Annual Project Review, DOE report 2013.
[8] J.C. Corelli, Knolls Atomic Power Lab., Schenectady, N.Y., 1960.

[9] G. R. Kilp, P. V. Mitchell, Westinghouse, United States Atomic Energy Commission 1961.
[10] R.A. Kubiak, E.H.C. Parker, R.M. King, K. Wittmaack, J. Vac. Sci. Technol., A 1 (1) (1983) 34–40.
[11] S. Budak, S. Guner, C. Muntele, D. Ila, Nucl Instrum Meth B 267 (2009) 1592.
[12] S. Budak, C. Smith, M. Pugh, K. Heidary, T. Colon, R.B. Johnson, C. Muntele, D. Ila, Radiat. Phys. Chem. 81 (2012) 410.
[13] S. Guner, S. Budak, C. Muntele, D. Ila, Surf Coat Tech 203 (2009) 2664.
[14] B. Zheng, Z. Xiao, B. Chhay, R. Zimmerman, D. Ila, Nucl Instrum Meth B 266 (2008) 73.
[15] B. Zheng, Z. Xiao, B. Chhay, R.L. Zimmerman, M.E. Edwards, D. Ila, Surf Coat Tech 203 (2009) 2682.
[16] G. Busch, U. Winkler, Helv. Phys. Acta 26 (1953) 395.
[17] C. Jacoboni, E.W. Prohofsk, Phys. Rev. B: Solid State 1 (1970) 697.
[18] R. Venkatasubramanian, T. Colpitts, B. O'Quinn, S. Liu, N. El-Masry, M. Lamvik, Appl. Phys. Lett. 75 (1999) 1104.
[19] H. Scherrer, S. Scherrer, in: D.M. Rowe (Ed.), CRC Press, Boca Raton, FL, 1995.
[20] N.D Arora, J.R. Hauser, D.J. Roulston, IEEE Trans. Electron Devices 29 (1982) 292.